PCCP

PAPER

View Article Online
View Journal | View Issue

Check for updates

Cite this: *Phys. Chem. Chem. Phys.*, 2022, **24**, 5211

Solving the discrepancy between the direct and relative-rate determinations of unimolecular reaction kinetics of dimethyl-substituted Criegee intermediate $(CH_3)_2COO$ using a new photolytic precursor†

Jari Peltola, Prasenjit Seal, Niko Vuorio, Petri Heinonen and Arkke Eskola*

Received 22nd May 2021,
Accepted 25th January 2022

DOI: 10.1039/d1cp02270a

rsc.li/pccp

We have performed direct kinetic measurements of the thermal unimolecular reaction of $(CH_3)_2COO$ in the temperature range 243–340 K and pressure range 5–350 Torr using time-resolved UV-absorption spectroscopy. We have utilized a new photolytic precursor, 2-bromo-2-iodopropane ($(CH_3)_2CIBr$), which photolysis at 213 nm in the presence of O_2 produces acetone oxide, $(CH_3)_2COO$. The results show that the thermal unimolecular reaction is even more important main loss process of $(CH_3)_2COO$ in the atmosphere than direct kinetic studies have suggested hitherto. The current experiments show that the unimolecular reaction rate of $(CH_3)_2COO$ at 296 K and atmospheric pressure is $899 \pm 42\ s^{-1}$. Probably more importantly, current measurements bring the direct and relative-rate measurements of thermal unimolecular reaction kinetics of $(CH_3)_2COO$ into quantitative agreement.

Introduction

Gas-phase ozonolysis is one of the major degradation pathways of biogenic and anthropogenic alkenes in the atmosphere. In ozonolysis, O_3 reacts with a double bond of an alkene forming a highly excited primary ozonide, which subsequently decomposes to an aldehyde and a Criegee intermediate. Depending on alkene and reaction conditions in the gas phase, a significant fraction of Criegee intermediates is often thermalized, producing stabilized Criegee intermediates (sCIs).[1] The impact of sCIs on atmospheric chemistry depends on their lifetime with respect to unimolecular reactions as well as on their bimolecular reactivity toward atmospheric trace species. The reactions of sCIs are sources of hydroxyl radicals (OH), organic acids, hydroperoxides, and aerosols in the troposphere.[2–6] In particular, the competition between the unimolecular and bimolecular reactions (mainly with water and SO_2) of sCIs play an important role since the oxidation of SO_2 by sCIs can be a significant source of sulfuric acid in alkene-rich environments.[7]

Acetone oxide, $(CH_3)_2COO$, is produced in the ozonolysis of isobutene[4] and any larger alkene with an $R_1R_2C{=}C(CH_3)_2$ moiety, such as trimethylethylene,[4] tetramethylethylene,[4,8] terpinolene,[9] and β-myrcene.[10] Hitherto, direct kinetic studies have shown that acetone oxide reacts quickly with SO_2,[11,12] but slowly with water monomer and dimer.[12,13] The slow reaction with water suggests that $(CH_3)_2COO$ can survive in high humidity conditions and may have a role in the atmospheric oxidation of SO_2. However, kinetic measurements indicate that the unimolecular reaction (R1) is fast enough to act as the dominant sink of $(CH_3)_2COO$ in the atmosphere.[11,13–15] According to a theoretical study by Long *et al.*,[16] the thermal unimolecular reaction of $(CH_3)_2COO$ is the dominant atmospheric sink above a temperature of 240 K, while the $(CH_3)_2COO + SO_2$ reaction can compete with it below 240 K using typical rural $[SO_2] = 9 \times 10^{10}$ molecules cm^{-3}.

$$(CH_3)_2COO \rightarrow \text{Products} \qquad \text{(R1)}$$

However, there is a consistent discrepancy between the direct and relative-rate thermal unimolecular reaction rate determinations of $(CH_3)_2COO$.[17] Smith *et al.*[14] and Chhantyal-Pun *et al.*[11] have performed direct kinetic measurements of the unimolecular reaction rate coefficient (k_{uni}) of $(CH_3)_2COO$ and

---

Department of Chemistry, University of Helsinki, P.O. Box 55 (A.I. Virtasen aukio 1), Helsinki, FI-00014, Finland. E-mail: arkke.eskola@helsinki.fi

† Electronic supplementary information (ESI) available: The determination of the effective optical path length and the $[(CH_3)_2COO]_0$, synthesis of the 2-bromo-2-iodopropane precursor, heating and cooling methods of the reactor, determination of k_{uni}, UV-spectra and cross-sections, comparison with the previous k_{uni} kinetic simulations, MESMER input files, and MESMER simulation results in ChemKin PLOG format. See DOI: 10.1039/d1cp02270a

obtained rates of 361 ± 49 s^{-1} at 298 K and 305 ± 70 s^{-1} at 293 K, respectively. In the study by Smith *et al.*,[14] k_{uni} shows a strong temperature dependence, increasing from 269 ± 82 s^{-1} at 283 K to 916 ± 56 s^{-1} at 323 K with an Arrhenius activation energy of ~25 kJ mol^{-1}. In turn, the relative-rate (k_{uni}/k_{SO_2}) determinations from ozonolysis studies of tetramethylethylene by Newland *et al.*[13] and Berndt *et al.*[15] result in k_{uni} values of 929 ± 220 s^{-1} at 298 K and 722 ± 52 s^{-1} at 293 K, respectively. These k_{uni} values are determined using the current (IUPAC) recommendation for the bimolecular $(CH_3)_2COO + SO_2$ reaction rate coefficient (k_{SO_2}).[17] Note that rates from relative-rate determinations appear to be *faster* than rates from direct measurements under the same conditions; the k_{uni} values from relative-rate determinations are about a factor of two larger than those from the direct kinetic measurements. The origin of this discrepancy is currently unclear.[17] The temperature dependences of k_{uni} reported by Berndt *et al.*[15] and Smith *et al.*[14] are similar. Smith *et al.*[14] also stated that the unimolecular decomposition of $(CH_3)_2COO$ is independent of pressure in the range of 100–200 Torr. Master equation (ME) simulations of the unimolecular decomposition of $(CH_3)_2COO$ performed by Fang *et al.*[18] suggest that at 300 K, k_{uni} is well within 10% of its high-pressure limit value at 10 Torr and 0.5% at 760 Torr of air.

Recently, we introduced and utilized a new photolytic precursor, CH_2IBr, which photolysis at 213 nm in the presence of O_2 produces CH_2OO.[19] This precursor was found to be more stable than CH_2I_2 against secondary reaction chemistry, which may regenerate CH_2OO in measurements and thus distort the kinetic data, especially in thermal unimolecular reaction rate experiments. Here we report a detailed study of the thermal unimolecular reaction kinetics of $(CH_3)_2COO$ over wide ranges of pressure (5–350 Torr) and temperature (243–340 K) using a new photolytic precursor, 2-bromo-2-iodopropane, $(CH_3)_2CIBr$. We also conducted ME simulations of the unimolecular reaction kinetics of $(CH_3)_2COO$. Finally, we compare the current results with previous determinations of $(CH_3)_2COO$ unimolecular reaction kinetics.

Experimental

Experiments were performed using a time-resolved, broadband, cavity-enhanced absorption spectrometer (TR-BB-CEAS) apparatus that is schematically shown in Fig. 1 and has been described previously.[19] Acetone oxide was produced homogeneously along the reactor by photolysis of $(CH_3)_2CIBr$ at 213 nm in the presence of O_2 ($[O_2] \gg [(CH_3)_2CI]$).

$$(CH_3)_2CIBr + h\nu(213\ \text{nm}) \rightarrow (CH_3)_2CI + Br \qquad (R2a)$$

$$\rightarrow \text{Other products} \qquad (R2b)$$

followed by

$$(CH_3)_2CI + O_2 \rightarrow (CH_3)_2COO + I \qquad (R3a)$$

$$\rightarrow \text{Other products} \qquad (R3b)$$

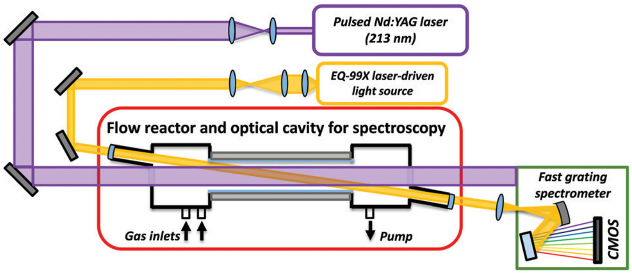

Fig. 1 Schematic figure of the time-resolved, broadband, cavity-enhanced absorption spectrometer. The sCI is produced along a heated or cooled flow tube reactor by a single-pass photolysis laser pulse at 213 nm. The sCI is probed by an overlapping incoherent laser-driven broadband light source. The sensitivity of the detector is enhanced using an optical cavity formed by two highly reflecting concave mirrors between 300 and 450 nm. The time-dependent broadband absorption spectrum of [sCI] is measured by a grating spectrometer combined with a fast CMOS line array camera.

The $(CH_3)_2CIBr$ precursor is not commercially available and was consequently synthesized in this work. The only method we managed to find from the literature[20] to synthesize 2-bromo-2-iodopropane is from the year 1878 and produces mainly 2,2-diiodopropane and only traces of the mixed halide. However, the addition of iodide to 2-bromopropene gives pure 2-bromo-2-iodopropane, if the reaction is carried out in an acid with a non-nucleophilic conjugate base, and the reaction is stopped when approximately 50% conversion is reached. We used trifluoroacetic acid as the solvent and potassium iodide as the iodide source (see more details in the ESI†). NMR analysis showed that the residual trifluoroacetic acid concentration in the precursor was < 0.01 wt%, resulting in $[CF_3COOH]_{max} < 2 \times 10^{10}$ molecules cm^{-3} in the reactor at the highest $[(CH_3)_2CIBr] = 6.3 \times 10^{13}$ molecules cm^{-3} used. This small residual $[CF_3COOH]$ had a negligible (<15 s^{-1}) effect on the kinetics of $(CH_3)_2COO$.

The premixed gas mixture flowing through the reactor contained the radical precursor $(CH_3)_2CIBr$ and O_2 diluted in helium or nitrogen carrier gas. All the gases were pre-heated or pre-cooled close to the setpoint temperature before flowing into the temperature-controlled reactor (see more details in the ESI†). The linear gas flow speed was about 1 ms^{-1}, ensuring that the gas mixture was completely replaced between photolysis laser pulses with a repetition rate of 1 Hz. The complete axial temperature profile within the overlap volume of the probe and the photolysis beams was measured separately for all experimental conditions (temperature, pressure, and flow rate) used in this work. The observed temperature 2σ-uncertainty in the measurement range 243–340 K was ≤ ±1.2 K.

All the kinetic traces of $(CH_3)_2COO$ were measured at 338 nm, which is close to the UV absorption maximum of $(CH_3)_2COO$.[21] The initial $[(CH_3)_2COO]_0$ was varied by adjusting $[(CH_3)_2CIBr]_0$. $[(CH_3)_2COO]_0$ was calculated from the peak absorbance using the absorption cross-section of $(CH_3)_2COO$ and the effective optical path length at the 338 nm wavelength used (see more details in the ESI†). For the experiments described here, we averaged the signal between 1000 and 9000 shots for each decaying experimental time-trace. The time–traces were probed with a time resolution of 67 μs.

Theoretical methods

In order to theoretically understand the effect of helium and nitrogen bath-gas pressures on k_{uni}, we performed quantum chemistry calculations and master equation simulations using the MESMER 6.0 program.[22] The geometry optimization and vibrational frequency calculations of the stationary points on the potential energy surface (PES) were performed using Truhlar's Minnesota functional, MN15[23] and def2-TZVP basis set as implemented in Gaussian 16 program.[24] The energies of the stationary points were then refined with the coupled cluster method, CCSD(T) as employed in ORCA code[25] and extrapolated to the complete basis set limit (CBS) using Dunning's correlation consistent basis sets, *i.e.*, cc-pVXZ (X = T and Q) following the scheme proposed by Neese and Valeev.[26]

$$E^{\mathrm{CBS}}_{\mathrm{total}}(X,X+1) \approx E^{\mathrm{CBS}}_{\mathrm{SCF}}(X,X+1) + E^{\mathrm{MDCI;CBS}}_{\mathrm{corr}}(X,X+1) \qquad (1)$$

The unimolecular reaction of $(CH_3)_2COO$ is believed to proceed through 1,4-hydrogen transfer from one of the $-CH_3$ groups to O–O to from methyl–vinyl hydroperoxide (Methyl-VHP) that may, depending on conditions, subsequently decompose to methyl–vinoxy and OH radicals.[16] The energy for TS2 (see Fig. 6) was taken from the study by Taatjes *et al.*[27]

For well-defined transition states, RRKM theory was used along with Eckart tunnelling corrections to calculate microcanonical rate coefficients. It is noteworthy that tunnelling is very important in the current case. For collisional energy transfer, a temperature-dependent exponential-down model was used.

$$\langle \Delta E \rangle_{\mathrm{down}} = \langle \Delta E \rangle_{\mathrm{down,298K}}(T/298\ \mathrm{K})^n \qquad (2)$$

Here, $\langle \Delta E \rangle_{\mathrm{down,298K}}$ is the collision energy transfer parameter at 298 K and its temperature dependency is governed by n. The terms $\langle \Delta E \rangle_{\mathrm{down,298K}}$ and n were optimized to get the best agreement between calculated and experimental rate coefficients. MESMER uses the Lennard–Jones (LJ) model for calculating the collisional frequency and requires the depth of the potential well, $\varepsilon_{\mathrm{LJ}}$, and the finite length where the potential is zero, σ_{LJ}.

Results and discussion

Experiments

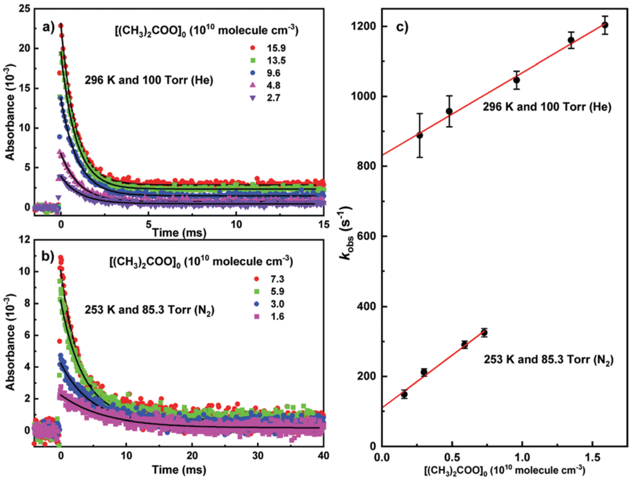

Fig. 2 The decay trace of $(CH_3)_2COO$ for various initial $[(CH_3)_2COO]_0$ at (a) 296 K and 100 Torr (He), and at (b) 253 K and 85.3 Torr (N_2). The $(CH_3)_2COO$ traces were probed at 338 nm with a time resolution of 67 μs. Black curves are the first-order exponential fits to the trace. (c) Obtained first-order rate coefficients (k_{obs}) from the presented exponential fits as a function of $[(CH_3)_2COO]_0$. Red lines are the linear least squares fits to the data. The statistical uncertainties shown are 2σ.

Fig. 2 shows typical decay traces of $(CH_3)_2COO$ obtained at various initial concentrations of $(CH_3)_2COO$ under two different temperature and pressure conditions. The measured transient signal of $(CH_3)_2COO$ mainly contains contributions from the thermal unimolecular reaction and the self-reaction, but also a small contribution from the gas diffusion loss and to some small extent from the possible reaction of $(CH_3)_2COO$ with other reactive species such as the iodine atom. A detailed rate equation for the process is presented in eqn (S4) (ESI†). As shown in Fig. 2, the decay rate of $(CH_3)_2COO$ is faster with higher $[(CH_3)_2COO]_0$ principally due to the self-reaction. Nonetheless, all the experimental $(CH_3)_2COO$ traces were modeled with a simplified rate equation[14] (eqn (S5), ESI†) and fitted using a first-order, single-exponential decay function.

$$A_t = A_0 \times \exp(-k_{\mathrm{obs}}) + A_{\mathrm{offset}} \qquad (3)$$

where k_{obs} is the obtained first-order decay rate coefficient, A_t is the absorbance at time t, A_0 is the initial absorbance (at time t = 0), and A_{offset} is the constant absorbance caused by non-reactive species (formed at time t = 0). The single-exponential function fits reasonably well with the absorption traces, although the observed absorbance can be slightly higher than the fitted value just after the photolysis. In addition, a constant positive baseline offset was observed, especially in the kinetic measurements above room temperature (see Fig. 2a). The baseline offset has been taken into account in the fittings using eqn (S3) (see more details in the ESI†).

In Fig. 2c are presented the obtained first-order decay rate coefficients (k_{obs}) as a function of $[(CH_3)_2COO]_0$ under two different temperature and pressure conditions. The linear relationship of k_{obs} with respect to $[(CH_3)_2COO]_0$ indicates that the reactive species, as well as $(CH_3)_2COO$, are formed at concentrations proportional to $[(CH_3)_2CIBr]_0$ in the photolysis (see more details in the ESI†). Extrapolating the k_{obs} to zero $[(CH_3)_2COO]_0$ removes the effect of radical–radical processes, such as the self-reaction. Hence, the unimolecular reaction rate coefficient of $(CH_3)_2COO$ can be determined from the intercept (k_{ic}) of the linear least squares fit to the obtained kinetic data.

We also tested the possible importance of the $(CH_3)_2COO$ + $(CH_3)_2CIBr$ reaction by performing experiments with higher precursor concentration, but with correspondingly lower laser

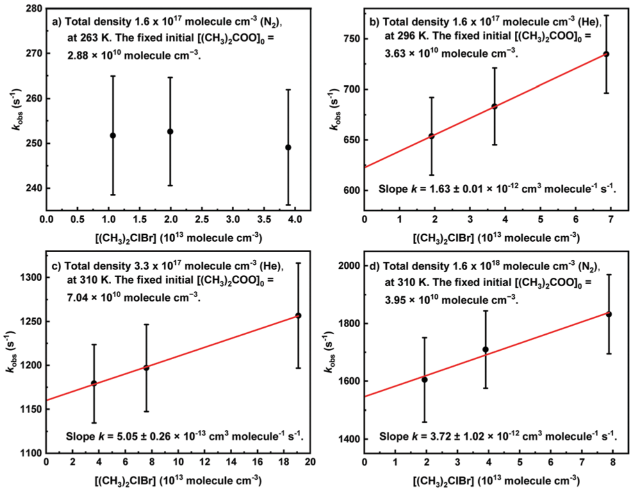

Fig. 3 Observed first-order rate coefficients of $(CH_3)_2COO$ as function of $(CH_3)_2ClBr$ concentration under different temperature and total density conditions. The fixed initial $(CH_3)_2COO$ concentration was (a) 2.88×10^{10} molecules cm^{-3}, (b) 3.63×10^{10} molecules cm^{-3}, (c) 7.04×10^{10} molecules cm^{-3}, and (d) 3.95×10^{10} molecules cm^{-3}. The $(CH_3)_2COO$ traces were probed at 338 nm. The statistical fitting uncertainties shown are 2σ.

fluence. The observed first-order decay rate coefficients are shown in Fig. 3 as function of $[(CH_3)_2ClBr]$ under various temperature and pressure conditions. At 263 K, the observed rate coefficients do not depend on $[(CH_3)_2ClBr]$ to any significant extent. However, at higher temperatures the decay of $(CH_3)_2COO$ becomes slightly faster at higher $[(CH_3)_2ClBr]$. All the measurements were performed under pseudo-first-order conditions, *i.e.* $[(CH_3)_2COO] \ll [(CH_3)_2ClBr]$. The bimolecular rate coefficients $k((CH_3)_2COO + (CH_3)_2ClBr)$ presented in Fig. 3 are obtained from the slope of the equation $k_{obs} = k_{loss} + k((CH_3)_2COO + (CH_3)_2ClBr) \times [(CH_3)_2ClBr]$ fitted to the data, while the intercept reflects k_{loss}.

Since the observed rate coefficients depend on $[(CH_3)_2ClBr]$ at higher temperatures, we performed an additional analysis to confirm that the precursor $(CH_3)_2ClBr$ (or impurities) does not affect the determination of k_{ic}. The following model was fitted to the observed k_{obs}-values under all T and p conditions

$$k_{obs} = k_{ic(3D)} + k_{sCI} \times [(CH_3)_2COO]_0 + k_P \times [(CH_3)_2ClBr] \qquad (4)$$

where, $k_{ic(3D)}$ is the intercept of the three-dimensional fit, k_{sCI} is the effective loss rate coefficient due to reactions of species with concentrations proportional to that of sCI, and k_P is the effective loss rate coefficient due to reactions of species with concentrations proportional to that of the precursor. The complete results of the $k_{ic(3D)}$-values fitted with eqn (4) are presented in Tables 1 and 2. The $k_{ic(3D)}$-values obtained with this method are very similar to the k_{ic}-values obtained with the two-dimensional model. Therefore, we conclude that the precursor or impurities in the precursor sample do not interfere with our kinetic analysis.

As mentioned above, the intercept (k_{ic}) of the linear least squares fit to the obtained kinetic data (Fig. 2c) includes the k_{uni} of $(CH_3)_2COO$, but also the diffusion loss (k_{loss}) originating from diffusion out of the measurement volume. To determine the k_{loss} of the current system, we measured the diffusion loss of CH_2OO under the same experimental conditions with the TR-BB-CEAS-apparatus (see more details in the ESI†). The thermal unimolecular decomposition rate coefficient of CH_2OO is negligible below a temperature of 375 K.[19,28] Approximating the diffusivities of CH_2OO and $(CH_3)_2COO$ with those of HCOOH and $CH_3(CH_3)CHCOOH$,[29] we obtain $k_{uni} = k_{ic}((CH_3)_2COO) - k_{loss}((CH_3)_2COO) = k_{ic}((CH_3)_2COO) - D(CH_3(CH_3)CHCOOH)/D(HCOOH) \times k_{loss}(CH_2OO) = k_{ic}((CH_3)_2COO) - 0.52 \times k_{loss}(CH_2OO)$ at a given temperature and total density. Fig. 4 shows the determined thermal unimolecular reaction rate coefficients of $(CH_3)_2COO$ as a function of helium buffer-gas pressure in the temperature range of 296–340 K. The complete kinetic results are shown in Table 1. Correspondingly, Fig. 5 and Table 2 show the results as a function of nitrogen buffer-gas pressure in the temperature range of 243–310 K.

The absorption cross-section of acetone oxide determined in this work from the measured spectrum between 320 and 400 nm and using Huang *et al.*'s[12,21] absolute value at 340 nm is shown in Fig. 6 along with the absorption cross-sections reported elsewhere. The low transmission of light through the optical cavity mirrors inhibits accurate measurements around 347 nm and at short wavelengths (*i.e.* $\leq$ 320 nm, see Fig. S5–S10, ESI†). The typical $[(CH_3)_2COO]$ used in the kinetic measurement was an order of magnitude lower than the $[(CH_3)_2COO] = 5.5 \times 10^{10}$ molecules cm^{-3} used in the measurement of the spectrum shown in Fig. 6. A fit to the original spectrum returned $[IO] \approx 2 \times 10^{10}$ molecules cm^{-3} (see ESI†), while the IO radical contribution has been removed from the Fig. 6 spectrum. Observed IO may have formed, for example, in reaction R3b.

The statistical fitting uncertainties shown in this study are 2σ. This includes uncertainties of all the measured exponential decays (k_{obs} and k_{uni}) and linear least squares fits. The estimated overall uncertainty in the measured unimolecular rate coefficients is ±20%.

Master equation analysis

The PES used in this work is shown in Fig. 7 with the value for TS2 taken from the study by Taatjes *et al.*[27] In the MESMER simulations of the unimolecular reaction of acetone oxide, only the channel shown in green in Fig. 7 was used, since it was observed that other channels are of negligible importance.[11,14] The LJ parameters in our calculations, σ = 4.46 Å and ε = 382.7 K, were taken from Long *et al.*[16] Fitting of the $\langle \Delta E \rangle_{down,298K}$ and n parameters to the experimental rate data was done using the Levenberg–Marquardt algorithm as implemented in MESMER, resulting the following collisional energy transfer expressions.

$$\langle \Delta E \rangle_{down} = 91.4 \times (T/298\ K)^{0.99} \quad \text{(He bath gas)}$$

$$\langle \Delta E \rangle_{down} = 212.4 \times (T/298\ K)^{0.7} \quad (N_2 \text{ bath gas})$$

The returned parameters of fittings are in a reasonable range. To obtain good agreement with the measured k_{uni}(He) and $k_{uni}(N_2)$ values presented in Fig. 4 and 5 and also given in

Table 1 Unimolecular reaction rate coefficients of $(CH_3)_2COO$ determined from the UV experiments in helium. k_{ic} is the intercept of the linear least squares fit to the observed kinetic data (k_{obs}) measured as a function of $[(CH_3)_2COO]$, with 2σ statistical fitting uncertainties. k_{uni} are derived as $k_{uni} = k_{ic} - k_{loss}$, where k_{loss} is $0.52 \times k_{loss}(CH_2OO)$ at a given temperature and total density (see more details in the ESI). $k_{uni,\ MESMER}$ are the results of MESMER simulations. High-pressure limiting rate coefficients ($p = \infty$) are taken from MESMER simulations at p = 10 atm. $k_{ic(3D)}$ is the intercept of the three-dimensional least squares fit (eqn (4)) to the observed kinetic data (k_{obs}), with 2σ statistical fitting uncertainties

T (K)	[He] ($\times 10^{18}$ molecules cm^{-3})	p^a (Torr)	k_{ic} (s^{-1})	k_{loss} (s^{-1})	k_{uni} (s^{-1})	$k_{uni,MESMER}$ (s^{-1})	$k_{ic(3D)}$ (s^{-1})
296	0.16	5	566 ± 24	52	514	595	608 ± 61
	0.33	10	608 ± 28	32	576	647	637 ± 17
	1.6	50	733 ± 14	15	718	747	722 ± 7
	3.3	100	826 ± 22	12	814	778	826 ± 37
	6.5	200	870 ± 22	10	860	802	850 ± 10
		∞				846	
310	0.16	5.2	884 ± 34	52	832	996	866 ± 50
	0.33	10.5	951 ± 60	32	919	1112	956 ± 110
	1.6	52.3	1354 ± 30	15	1339	1351	1347 ± 43
	3.3	104.8	1416 ± 54	12	1404	1434	1430 ± 79
	6.5	209.5	1575 ± 162	10	1565	1499	1556 ± 151
		∞				1627	
323	0.16	5.5	1168 ± 180	52	1116	1575	1553 ± 529
	0.33	10.9	1591 ± 148	32	1559	1803	1776 ± 217
	1.6	54.5	2346 ± 50	15	2331	2307	2340 ± 93
	3.3	109	2489 ± 44	12	2477	2492	2731 ± 201
	6.5	218	2925 ± 86	10	2915	2647	2989 ± 101
		∞				2971	
330	0.16	5.6	1566 ± 24	52	1514	1996	1575 ± 23
	0.33	11.2	2066 ± 122	32	2034	2317	2108 ± 107
	1.6	55.7	3344 ± 84	15	3329	3052	3353 ± 204
	3.3	111.5	3333 ± 150	12	3321	3333	3826 ± 119
		∞				4090	
340	0.16	5.8	1660 ± 104	52	1608	2770	1631 ± 130
	0.33	11.7	3003 ± 26	32	2971	3293	2998 ± 985
	1.6	57.5	4423 ± 422	15	4408	4503	4610 ± 352
		∞				6410	

[a] The fixed O_2 concentration was $\sim 4 \times 10^{16}$ molecules cm^{-3}.

Tables 1 and 2, we slightly tuned the barrier TS1 in Fig. 7 by making it 0.55 kJ mol^{-1} lower. This small adjustment to the transition-state energy is well within an expected uncertainty of the theoretical calculations.

Yields of the methyl–vinyl hydroperoxide and methyl–vinoxy + OH products under different experimental temperature and pressure conditions were (roughly) estimated in MESMER simulations. Simulations of experiments using helium bath gas were performed at 296 K and at four temperatures up to 340 K. As shown in Table S3 (ESI†), 1 second after reaction initiation, the yield of Methyl-VHP is 72% at 200 Torr pressure, showing significant stabilization to the well at 296 K. Upon increasing the temperature to 340 K, stabilization to the well becomes almost negligible. 500 Seconds after reaction initiation, all Methyl-VHP have decomposed to methyl-vinoxy + OH products at all temperatures and pressures. Simulations of experiments using nitrogen bath gas, which were also performed at temperatures well below 296 K, show that stabilization to the well 1 second after reaction initiation is significant at all experimental temperatures (*i.e.* $T \leq 310$ K). At longer times, Methyl-VHP again decomposes to methyl-vinoxy + OH products. However, these product yields are very sensitive to the energy of the TS2 and current experiments are only able to constrain the energy of the TS1. Still, these simulations show that while methyl-vinoxy + OH are probably the main atmospheric chemistry relevant products of the unimolecular reaction of $(CH_3)_2COO$, stabilization of methyl–vinyl hydroperoxide may also play a role. MESMER input files for the two bath gases are given in the ESI.†

Comparison with the previous kinetic determinations of R1

In Table 3, we compare the current results with previous experimental and theoretical works. The comparison shows that the current value of k_{uni} from our direct measurements is more than twice the previously reported values from the direct measurements of Smith *et al.*[14] and Chhantyal-Pun *et al.*[11] and the theoretical kinetics of reaction (1) by Long *et al.*,[16] all at room temperature. Note that both Smith *et al.*[14] and Chhantyal-Pun *et al.*[11] used a $(CH_3)_2CI_2$ photolytic precursor in their measurements. The difference in values of k_{uni} between our and Smith *et al.*'s[14] results is even larger at higher temperatures. Overall, the direct measurements of unimolecular rate coefficients of (R_1) by Smith *et al.* are about 65%–30% of our values in the temperature range 283–323 K. However, our room-temperature value of k_{uni} is in good agreement with the values of the unimolecular reaction rate coefficient of $(CH_3)_2COO$ from the relative-rate ozonolysis studies of tetramethylethylene by Berndt *et al.*[8] and Newland *et al.*[13] In addition, Fig. S11 (ESI†) shows a more detailed comparison between our results and those of Long *et al.*[16] The unimolecular reaction rates of Long *et al.*[16] are about half our values at higher pressures, irrespective of the temperature.

Table 2 Unimolecular reaction rate coefficients of $(CH_3)_2COO$ determined from the UV experiments in nitrogen. k_{ic} is the intercept of the linear least squares fit to the kinetic data (k_{obs}) measured as a function of $[(CH_3)_2COO]$, with 2σ statistical fitting uncertainties. k_{uni} are derived as $k_{uni} = k_{ic} - k_{loss}$, where k_{loss} is $0.52 \times k_{loss}(CH_2OO)$ at a given temperature and total density (see more details in the ESI). $k_{uni,\ MESMER}$ are the results of MESMER simulations. High-pressure limiting rate coefficients ($p = \infty$) are taken from MESMER simulations at $p = 10$ atm. $k_{ic(3D)}$ is the intercept of the three-dimensional least squares fit (eqn (4)) to the observed kinetic data (k_{obs}), with 2σ statistical fitting uncertainties

T (K)	$[N_2]$ ($\times 10^{18}$ molecules cm^{-3})	p^a (Torr)	k_{ic} (s^{-1})	k_{loss} (s^{-1})	k_{uni} (s^{-1})	$k_{uni,MESMER}$ (s^{-1})	$k_{ic(3D)}$ (s^{-1})
243	0.16	4.1	91 ± 12	16	75	74	77 ± 12
	0.33	8.2	87 ± 8	10	77	74	94 ± 1
	1.6	41	68 ± 14	5	63	75	76 ± 33
	3.3	82	51 ± 16	4	47	75	56 ± 13
		∞				75	
253	0.16	4.3	118 ± 10	16	102	110	119 ± 5
	0.33	8.5	115 ± 10	10	105	112	115 ± 12
	1.6	42.6	118 ± 6	5	113	113	122 ± 14
	3.3	85.3	110 ± 26	4	106	114	107 ± 46
		∞				114	
263	0.16	4.4	163 ± 8	16	147	166	156 ± 9
	0.33	8.9	170 ± 16	10	160	169	169 ± 20
	1.6	44.3	153 ± 20	5	148	174	144 ± 23
	3.3	88.7	147 ± 18	4	143	175	141 ± 16
		∞				176	
273	0.16	4.6	239 ± 12	16	223	251	239 ± 24
	0.33	9.2	264 ± 46	10	254	259	265 ± 47
	1.6	46	262 ± 24	5	257	270	267 ± 37
	3.3	92.1	279 ± 6	4	275	272	278 ± 2
		∞				276	
283	0.16	4.8	337 ± 56	16	321	380	366 ± 65
	0.33	9.6	321 ± 40	10	311	396	255 ± 82
	1.6	47.8	449 ± 20	5	444	421	452 ± 22
	3.3	95.5	417 ± 48	4	413	428	364 ± 43
		∞				437	
296	0.16	5	605 ± 36	16	589	648	635 ± 39
	0.33	10	627 ± 62	10	617	688	683 ± 43
	1.6	50	856 ± 46	5	851	755	950 ± 235
	6.5	200	902 ± 42	3	899	785	880 ± 62
		∞				802	
310	0.33	10.5	1085 ± 120	10	1075	1229	1091 ± 381
	1.6	52.3	1355 ± 228	5	1350	1405	1170 ± 70
		∞				1548	

[a] The fixed O_2 concentration was ~4 × 10^{16} molecules cm^{-3}.

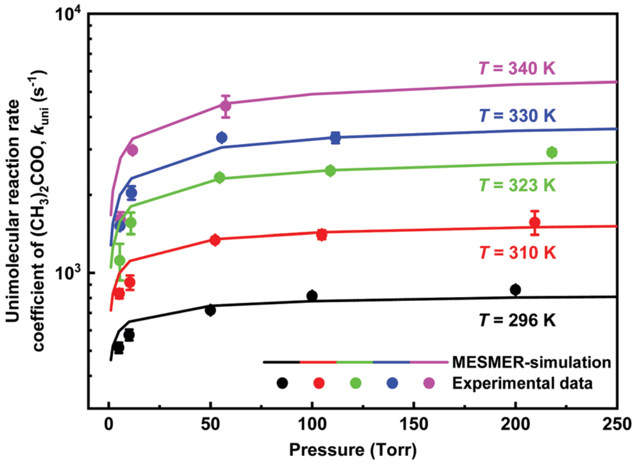

Fig. 4 Measured thermal unimolecular reaction rate coefficient of $(CH_3)_2COO$ as a function of total (mainly helium) pressure at different temperatures (coloured points). The statistical uncertainties shown are 2σ. Results of MESMER simulations (solid lines) are also shown.

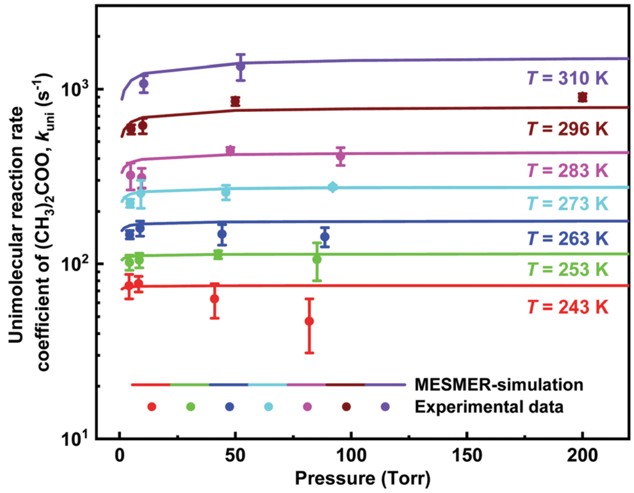

Fig. 5 Measured thermal unimolecular reaction rate coefficient of $(CH_3)_2COO$ as a function of total (mainly nitrogen) pressure at different temperatures (coloured points). The statistical uncertainties shown are 2σ. Results of MESMER simulations (solid lines) are also shown.

A probably more revealing comparison is shown in Fig. 8, where an Arrhenius plot of the current k_{uni} values from 100 Torr

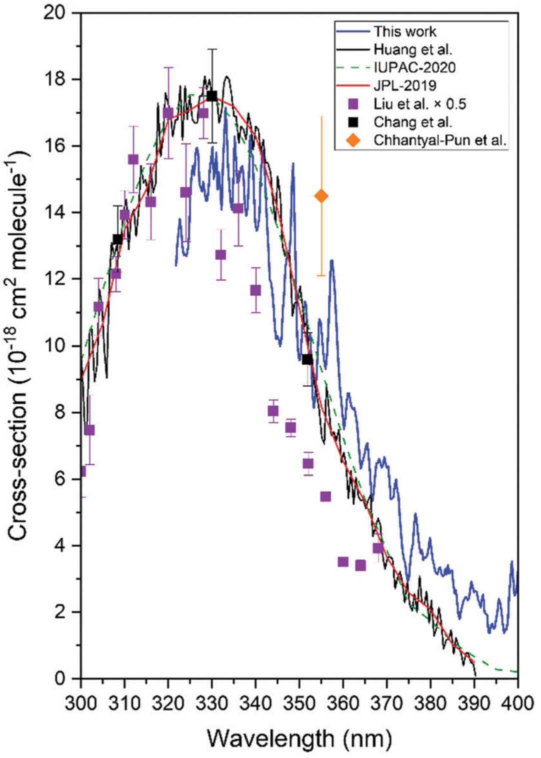

Fig. 6 Absorption spectrum of $(CH_3)_2COO$ measured at 296 K temperature and 10 Torr pressure using $(CH_3)_2CIBr$ photolytic precursor. The spectrum was obtained by averaging over t = 0–1 ms after photolysis initiation and $[(CH_3)_2COO]_0$ was 5.5 × 10^{10} molecules cm^{-3} in these measurements. Absorption spectra reported by other groups are shown for comparison.[11,12,21,30–32]

measurements (corresponding approximately to the high-pressure limit of k_{uni}) is shown with the results of previous temperature-dependent k_{uni} studies by Berndt *et al.*,[8] Long *et al.*,[16] and Smith *et al.*[14] It is evident from Fig. 8 that the current measurements agree quantitatively with Berndt *et al.*'s[8] results over a wide temperature range, whereas both show clearly faster unimolecular kinetics than k_{uni} determinations at the high-pressure limit by Long *et al.*[16] and Smith *et al.*[14] The temperature dependency (and activation energy) of k_{uni} observed in this work closely resemble those reported in the Berndt *et al.*[8] and Long *et al.*[16] studies. However, the temperature dependency of k_{uni} obtained by Smith *et al.*[14] in their direct measurements using a $(CH_3)_2CI_2$ photolytic precursor is clearly smaller than in the other three studies. We suggest that both the smaller values of k_{uni} obtained by Smith *et al.*[14] and Chhantyal-Pun *et al.*[11] at room temperature as well as the weaker temperature dependency shown by Smith *et al.*[14] than that observed in the current study, originate from the use of a $(CH_3)_2CI_2$ photolytic precursor and some undisclosed reaction that produces $(CH_3)_2COO$ during the kinetic experiments. This $(CH_3)_2COO$ recycling then distorts the results, giving kinetics that are slower than in reality. We believe that, similar to our previous work,[19] our new photolytic precursor $(CH_3)_2CIBr$ is more stable against secondary chemistry since it does not produce $(CH_3)_2CI$ radicals and consequently $(CH_3)_2COO$ in the X + $(CH_3)_2CIBr$ → XI + $(CH_3)_2CBr$ reaction, where X is any species. Still, more work is needed to find out and quantify the underlying mechanism.

We do not believe that the new production method of $(CH_3)_2CI$ radical and subsequent acetone oxide introduced in this work has caused the faster unimolecular decays observed. Using bond dissociation energies of CH_3–Br (294 kJ mol^{-1})[33] and CH_3–I (239 kJ mol^{-1})[33] as well as the difference in energy between 213 and 248 nm photons (79.3 kJ mol^{-1}), a rough

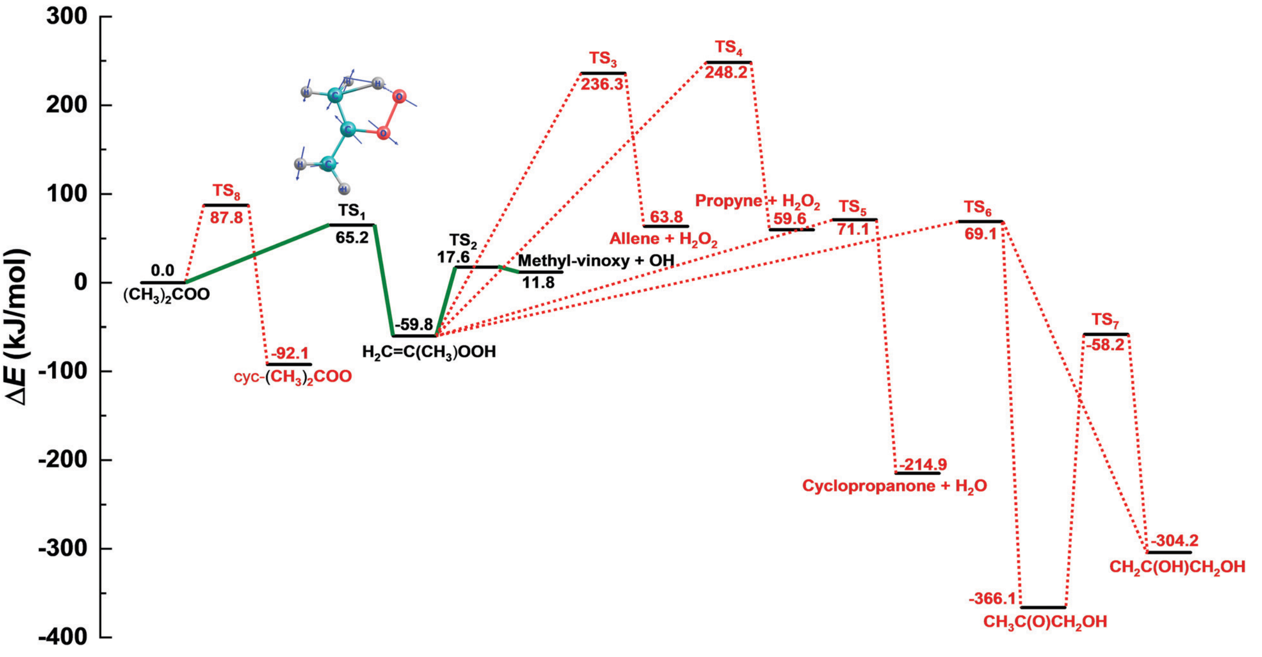

Fig. 7 Zero-point inclusive potential energy surface (PES) for the unimolecular reaction of acetone oxide in kJ mol^{-1}. We considered only the green channel in our MESMER simulations. The value for TS2 is taken from the study of Taatjes *et al.*[27]

Table 3 Summary of unimolecular reaction rate coefficients and Arrhenius activation energies of $(CH_3)_2COO$ reported in (or derived from) previous studies and this work

Ref.	Method	T (K)	p^a (Torr)	k_{uni} (s^{-1})	E_a (kJ mol^{-1})
This work	Direct experiment	253	85.3	106 ± 26	~32
Long *et al.*[16]	Theoretical calculation	250	99.8	40	~34
This work	Direct experiment	283	95.5	413 ± 48	~32
Smith *et al.*[14]	Direct experiment	283	200	269 ± 164	~25
Berndt *et al.*[8]	Relative-rate experiment	278	760	416 ± 121[b]	~29
This work	Direct experiment	296	200	899 ± 42	~32
Smith *et al.*[14]	Direct experiment	298	200	361 ± 98	~25
Chhantyal-Pun *et al.*[11]	Direct experiment	293	~100[c]	305 ± 70[c]	—
Berndt *et al.*[8]	Relative-rate experiment	293	760	722 ± 52[b]	~29
Newland *et al.*[13]	Relative-rate experiment	298	760	929 ± 220[b]	—
Long *et al.*[16]	Theoretical calculation	298	200	420	~34
This work	Direct experiment	323	218	2915 ± 86	~32
Smith *et al.*[14]	Direct experiment	323	200	916 ± 112	~25
Berndt *et al.*[8]	Relative-rate experiment	323	760	2449 ± 865[b]	~29
Long *et al.*[16]	Theoretical calculation	323	200	1376	~34

[a] The fixed O_2 concentration was $\sim 4 \times 10^{16}$ molecules cm^{-3}. [b] The k_{uni} value is derived from the reported relative-rate (k_{uni}/k_{SO_2}) using the current recommendation (IUPAC) for $k_{SO_2} = 4.23 \times 10^{-13} \exp(1760/T)$ cm^3 $molecule^{-1}$ s^{-1}.[17] [c] The reported value is the average of the first-order loss rate coefficient obtained in the pressure range of 10–100 Torr. At each pressure, the first-order loss rate coefficient was obtained from the simultaneous first- and second-order decay fits to the measured $(CH_3)_2COO$ decay traces. The uncertainties shown in Table 3 are 2σ.

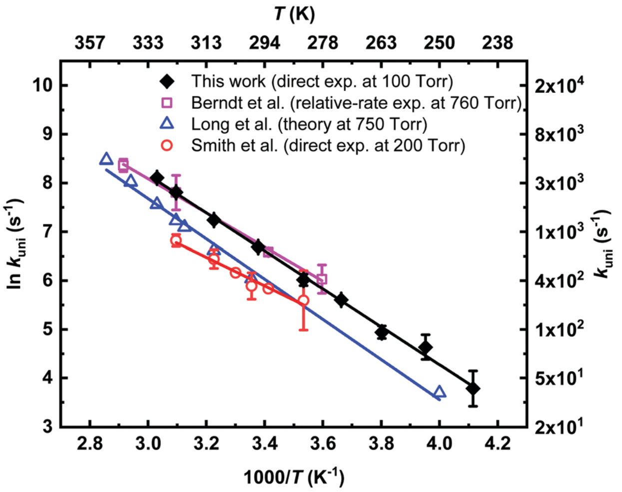

Fig. 8 An Arrhenius plot of the current unimolecular reaction rate coefficients of $(CH_3)_2COO$ from 100 Torr measurements (filled black diamonds) together with the previous studies of Berndt *et al.*[8] (open magenta squares), Long *et al.*[16] (open blue triangles), and Smith *et al.*[14] (open circles). Solid lines are the linear least-squares fits to the data. The least-squares fit to the current 100 Torr data gives an Arrhenius expression $k = (19.7 \pm 0.6) \times \exp[(-32.0 \pm 1.4)\ \mathrm{kJ\ mol^{-1}}/RT]\ s^{-1}$, with 2σ standard fitting uncertainties.

estimate of the additional energy imparted to $(CH_3)_2CI$ + Br products in 213 nm photolysis of $(CH_3)_2CIBr$ in comparison to $(CH_3)_2CI$ + I products in 248 nm photolysis of $(CH_3)_2CI_2$ is about 24 kJ mol^{-1}. This additional energy is small (<10%) in comparison to the total energy imparted to $(CH_3)_2CI$ + I products in 248 nm photolysis of $(CH_3)_2CI_2$ which is about 243 kJ mol^{-1} (estimating bond dissociation energy of $(CH_3)_2CI$–I with that of CH_3–I). The slightly higher internal energy of the $(CH_3)_2CI$ radical (+Br) immediately after photolysis may, at most, result in slightly higher IO production *via* channel R3b. We are also confident that our reactive species (*e.g.* $(CH_3)_2CI$, $(CH_3)_2COO$, and Br- and I-atoms) concentrations were low enough to avoid any importance of Criegee–Criegee, Criegee–radical and radical–radical reactions to the measured unimolecular kinetics. Due to the low $(CH_3)_2COO$ concentrations employed and their extrapolation to zero concentration (see Fig. 2), there is no need for a complicated model to fit the data.

Conclusions

This work introduces a new photolytic precursor for acetone oxide, 2-bromo-2-iodopropane, which photolysis at 213 nm in the presence of O_2 produces $(CH_3)_2COO$. Utilizing this new photolytic precursor we have performed direct unimolecular reaction rate measurements of $(CH_3)_2COO$ over a wide range of conditions and observed that the obtained kinetics is more than twice as fast at all temperatures as the previous direct kinetic measurements using a $(CH_3)_2CI_2$ photolytic precursor suggest. We believe that the current measurements using the $(CH_3)_2CIBr$ photolytic precursor are resistant to secondary chemistry that may lead to $(CH_3)_2COO$ formation *during* time-resolved measurements and thus distort experimental kinetic results. For this reason, the current values of k_{uni} are the preferred values for atmospheric *etc.* modelling. Our current and previous[19] measurements of sCI kinetics utilizing an R_1R_2CIBr precursor with 213 nm photolysis show that this is the preferable method of sCI production, especially in unimolecular reaction kinetic experiments of sCIs.

Conflicts of interest

Authors declare no conflicts of interest.

Acknowledgements

J. P., P. S., and N. V. acknowledge support from the Academy of Finland, Grant numbers 298910 and 311967. A. E.

acknowledges support from the Academy of Finland, Grant numbers 294042, 319353, and 288377. The financial support from the University of Helsinki is also acknowledged.

References

1 R. Criegee, *Angew. Chem.*, 1975, **14**, 745–752.

2 J. Tröstl, W. K. Chuang, H. Gordon, M. Heinritzi, C. Yan, U. Molteni, L. Ahlm, C. Frege, F. Bianchi and R. Wagner, *Nature*, 2016, **533**, 527–531.

3 C. A. Taatjes, *Annu. Rev. Phys. Chem.*, 2017, **68**, 183–207.

4 D. Johnson and G. Marston, *Chem. Soc. Rev.*, 2008, **37**, 699–716.

5 L. Vereecken, A. Novelli and D. Taraborrelli, *Phys. Chem. Chem. Phys.*, 2017, **19**, 31599–31612.

6 Z. Hassan, M. Stahlberger, N. Rosenbaum and S. Bräse, *Angew. Chem., Int. Ed.*, 2021, **60**, 2–17.

7 R. Mauldin Iii, T. Berndt, M. Sipilä, P. Paasonen, T. Petäjä, S. Kim, T. Kurtén, F. Stratmann, V. Kerminen and M. Kulmala, *Nature*, 2012, **488**, 193–196.

8 T. Berndt, T. Jokinen, R. L. Mauldin, T. Petäjä, H. Herrmann, H. Junninen, P. Paasonen, D. R. Worsnop and M. Sipilä, *J. Phys. Chem. Lett.*, 2012, **3**, 2892–2896.

9 Y. Ma and G. Marston, *Phys. Chem. Chem. Phys.*, 2009, **11**, 4198–4209.

10 P. Deng, L. Wang and L. Wang, *J. Phys. Chem. A*, 2018, **122**, 3013–3020.

11 R. Chhantyal-Pun, O. Welz, J. D. Savee, A. J. Eskola, E. P. Lee, L. Blacker, H. R. Hill, M. Ashcroft, M. A. H. Khan, G. C. Lloyd-Jones, L. Evans, B. Rotavera, H. Huang, D. L. Osborn, D. K. W. Mok, J. M. Dyke, D. E. Shallcross, C. J. Percival, A. J. Orr-Ewing and C. A. Taatjes, *J. Phys. Chem. A*, 2017, **121**, 4–15.

12 H. L. Huang, W. Chao and J. J. Lin, *Proc. Natl. Acad. Sci. U. S. A.*, 2015, **112**, 10857–10862.

13 M. J. Newland, A. R. Rickard, M. S. Alam, L. Vereecken, A. Munoz, M. Ródenas and W. J. Bloss, *Phys. Chem. Chem. Phys.*, 2015, **17**, 4076–4088.

14 M. C. Smith, W. Chao, K. Takahashi, K. A. Boering and J. J. Lin, *J. Phys. Chem. A*, 2016, **120**, 4789–4798.

15 T. Berndt, T. Jokinen, M. Sipilä, R. L. Mauldin III, H. Herrmann, F. Stratmann, H. Junninen and M. Kulmala, *Atmos. Environ.*, 2014, **89**, 603–612.

16 B. Long, J. L. Bao and D. G. Truhlar, *Proc. Natl. Acad. Sci. U. S. A.*, 2018, **115**, 6135–6140.

17 R. A. Cox, M. Ammann, J. N. Crowley, H. Herrmann, M. E. Jenkin, V. F. McNeill, A. Mellouki, J. Troe and T. J. Wallington, *Atmos. Chem. Phys.*, 2020, **20**, 13497–13519.

18 Y. Fang, F. Liu, V. P. Barber, S. J. Klippenstein, A. B. McCoy and M. I. Lester, *J. Chem. Phys.*, 2016, **144**, 061102.

19 J. Peltola, P. Seal, A. Inkilä and A. J. Eskola, *Phys. Chem. Chem. Phys.*, 2020, **22**, 11797–11808.

20 M. E. Reboul, *Ann. Chim.*, 1878, **5**, 477.

21 Y. Chang, C. Chang, K. Takahashi and J. J. Lin, *Chem. Phys. Lett.*, 2016, **653**, 155–160.

22 D. R. Glowacki, C. H. Liang, C. Morley, M. J. Pilling and S. H. Robertson, *J. Phys. Chem. A*, 2012, **116**, 9545–9560.

23 H. S. Yu, X. He, S. L. Li and D. G. Truhlar, *Chem. Sci.*, 2016, **7**, 5032–5051.

24 M. Frisch, G. Trucks, H. Schlegel, G. Scuseria, M. Robb, J. Cheeseman, G. Scalmani, V. Barone, B. Mennucci and G. Petersson, *Gaussian09, Revision D*, 2016.

25 F. Neese, *Wiley Interdiscip. Rev.: Comput. Mol. Sci.*, 2018, **8**, e1327.

26 F. Neese and E. F. Valeev, *J. Chem. Theory Comput.*, 2011, **7**, 33–43.

27 C. A. Taatjes, F. Liu, B. Rotavera, M. Kumar, R. Caravan, D. L. Osborn, W. H. Thompson and M. I. Lester, *J. Phys. Chem. A*, 2017, **121**, 16–23.

28 D. Stone, K. Au, S. Sime, D. Medeiros, J. M. Blitz, P. W. Seakins, Z. Decker and L. Sheps, *Phys. Chem. Chem. Phys.*, 2018, **20**, 24940–24954.

29 M. J. Tang, M. Shiraiwa, U. Pöschl, R. A. Cox and M. Kalberer, *Atmos. Chem. Phys.*, 2015, **15**, 5585–5598.

30 IUPAC Task Group on Atmospheric Chemical Kinetic Data Evaluation (The datasheet of interest last evaluated, 2020, (http://iupac.pole-ether.fr).

31 J. B. Burkholder, S. P. Sander, J. Abbatt, J. R. Barker, C. Cappa, J. D. Crounse, T. S. Dibble, R. E. Huie, C. E. Kolb, M. J. Kurylo, V. L. Orkin, C. J. Percival, D. M. Wilmouth and P. H. Wine, *Chemical Kinetics and Photochemical Data for Use in Atmospheric Studies*, Jet Propulsion Laboratory, Pasadena, 2019, http://jpldataeval.jpl.nasa.gov.

32 F. Liu, J. M. Beames, A. M. Green and M. I. Lester, *J. Phys. Chem.*, 2014, **118**, 2298–2306.

33 Y.-R. Luo, *Handbook of Bond Dissociation Energies in Organic Compounds*, CRC Press, Boca Raton, Fla, 2003.